

The role of chain-end association lifetime in segmental and chain dynamics of telechelic polymers

Kunyue Xing^{1†}, Martin Tress^{1†}, Peng-Fei Cao^{2*}, Fei Fan¹, Shiwang Cheng³, Tomonori Saito², and Alexei P. Sokolov^{1, 2*}

[†] The two authors contributed equally to this work.

[*] Alexei P. Sokolov (sokolov@utk.edu), Peng-Fei Cao (caop@ornl.gov)

¹ *University of Tennessee Knoxville, Department of Chemistry, Knoxville, Tennessee 37996, United States*

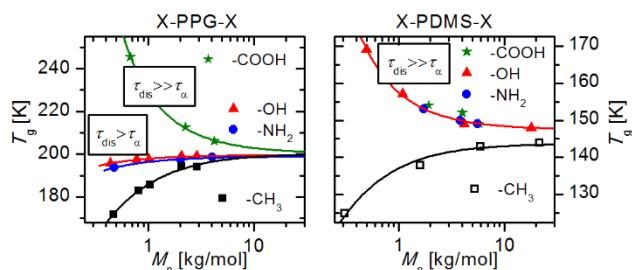
² *Oak Ridge National Laboratory, Chemical Sciences Division, Oak Ridge, Tennessee 37831, United States*

³ *Michigan State University, Department of Engineering, East Lansing, Michigan 48824, United States*

Abstract

Broadband dielectric spectroscopy, differential scanning calorimetry, and rheology were employed to study the impact of hydrogen (H) bonding end-groups on segmental and chain dynamics of telechelic polypropylene glycol (PPG) and poly(dimethylsiloxane) (PDMS). Polymer chains with three types of H-bonding end-groups possessing different interaction strength, and a non-H-bonding end-group as reference were compared. The glass transition temperature (T_g) of H-bonding PPG systems with low molecular weight increases compared to the reference, and the T_g difference varies with chain-end interaction strength. In contrast, their shear viscosities (for T_g -

scaled temperature, i.e. when the shift in T_g is accounted for) are similar to that one of the reference. This is in strong contrast to the behavior of telechelic PDMS with the same set of end-groups, where the T_g increase of all H-bonding systems is independent of H-bond strengths, while shear viscosity increases significantly only for the strongest H-bonding end-groups. These observations are explained by the difference in lifetime of the end-group associations relative to segmental and chain relaxation times.



For table of contents use only

1. Introduction.

Supramolecular polymers form an interesting class of materials with transient physical interactions,¹⁻⁵ such as hydrogen bonding⁶⁻¹⁹, metal complexation²⁰⁻²², ionic forces^{23, 24} and $\pi - \pi$ interactions.²⁵ These interactions can be controlled by temperature, pH, light irradiation or mechanical forces²⁶. They are promising candidates for functional materials such as, sensors²⁷, controlled release systems²⁸, self-healing^{19, 29-31} and shape-memory materials^{32, 33}. Due to its intrinsic directionality and variability of cohesive strength, hydrogen (H-) bonding is the most common and promising secondary interaction involved in the formation of supramolecular

polymers^{1,3}. The cohesive strength of H-bonding motifs can be adjusted by changing the number, geometry and specific chemistry of H-bonding units in the associating motifs³⁴⁻³⁷.

The application of supramolecular polymer networks usually involves their mechanical and viscoelastic properties, which can be tuned by modifying the interaction strength, morphology of the associating groups and the polymer architecture. Typically, dynamic bonds are generated in the melt which can behave like permanent bonds and form a network, e.g. at low temperature. Then, even low molecular weight (MW) polymers may display high viscosities similar to high MW systems. Different theoretical models, such as Cates entangled “living” polymers³⁸, sticky Rouse and sticky reptation model³⁹⁻⁴⁴ by Leibler, Rubinstein, Colby and Semenov, have been developed to understand the structure, dynamics and viscoelastic properties of such supramolecular polymer networks. These models focus on the impact of the lifetime of associating groups on the viscoelastic properties of a polymer. However, till now much less is known in both experiment and theory about changes of segmental dynamics in associating polymers.

Polypropylene glycol (PPG) is a common glass forming polymer that has been studied by different techniques such as dielectric spectroscopy⁴⁵⁻⁵², calorimetry⁵³, nuclear magnetic resonance (NMR)⁵⁴, mechanical experiments⁵⁵⁻⁵⁷, neutron scattering⁵⁸ and various light scattering methods⁵⁹⁻⁶¹. It is known that the glass transition temperature (T_g) of PPG with hydroxyl groups at both chain ends is almost independent of molecular weight⁶². On the contrary, Engberg et al.⁶⁰ found that the structural relaxation dynamics of methyl-terminated PPG exhibits a pronounced molecular weight dependence. Richter et al.⁶³ studied the association of heterocomplementary telechelic PPG, bearing either diaminotriazine (DAT) or thymine (Thy) stickers as end-groups that can produce 3 H-bonds each. From small angle neutron scattering (SANS), they concluded that linear association prevails in this system. Leibler et al.⁶⁴ presented results of telechelic supramolecular polymers

based on PPG with DAT/Thy functionalities on both ends (DAT-PPG-DAT, Thy-PPG-Thy). By comparing Thy/DAT self-association and complementary association, they concluded that complementary interactions can suppress mesoscopic order⁶⁵, thus leading to a counterintuitive change in material properties. The tendency of crystallization of the Thy and resulting phase segregation of the chain-ends makes the system more complicated. While these results reveal many details about the dynamics and network structures of PPG with different associating chain-ends, there is rather limited discussion of segmental dynamics in telechelic polymers and its role in the formation of supramolecular networks.

Here we present a combined study of segmental dynamics, glass transition and rheological properties of telechelic PPG with different strength of chain end interactions: methyl-terminated (PPG-CH₃), hydroxyl-terminated (PPG-OH), amine-terminated (PPG-NH₂) and carboxylic-terminated (PPG-COOH). Analysis of the data revealed significant influence of the chain end interaction strength on T_g at relatively low molecular weight. At the same time, viscosity appears to be almost independent of the chain-end interactions once the shift of T_g is accounted for (presented vs temperatures scaled by T_g). These results are in strong contrast to earlier studies of telechelic PDMS with the same set of chain ends.^{66, 67} In the case of telechelic PDMS the increase in T_g is independent of the strength of the chain-end H-bonding, while viscosity varies drastically (even plotted vs T/T_g). Based on these contrasting results, we propose a qualitative explanation considering the lifetime of chain-end dissociation in comparison to the characteristic chain and segmental relaxation time. If the dissociation time is much longer than the segmental time, T_g appears to reach some limiting value with no significant dependence on the strength of the chain end association. However, if the dissociation time is shorter than the chain relaxation time, no

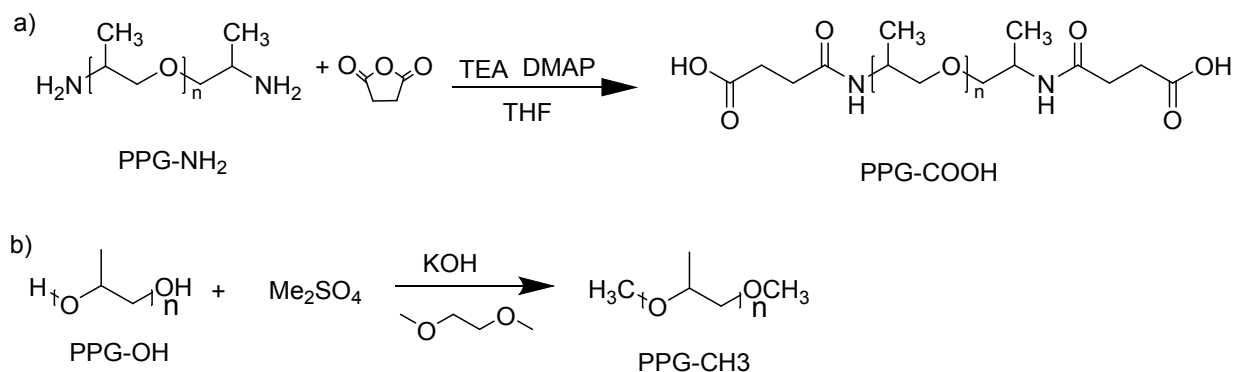
significant influence on viscosity is expected. Thus the ratio of characteristic time scales should be considered in the design of associating polymers in order to achieve the desired properties.

2. Material and methods.

2.1 Synthesis and Characterization. Polypropylene glycol (PPG-OH) with number averaged molecular weights (M_n) of 440, 846, 1078, 2180, and 3282 g/mol was received from Scientific Polymer Products, Inc. PPG bis(2-aminopropyl ether) (PPG-NH₂) with M_n of 480, 2046 and 4018 g/mol was purchased from Sigma-Aldrich and used directly without further purification (all M_n values given here were determined by ¹H NMR, see below). 4-(Dimethylamino) pyridine (DMAP), dimethyl sulfate and succinic anhydride were obtained from Sigma-Aldrich; ethylene glycol dimethyl ether was purchased from TGI; dichloromethane (DCM), methanol and hydrochloric acid (36.5-38%) were purchased from VMR Analytical and used as received. Triethylamine (TEA) was distilled under calcium hydride (CaH₂) before use. The different types of H-bonding end groups vary significantly in their MW. In order to compare systems of the same main chain length, we use the degree of polymerization (DP) based on M_n of the main chain rather than the total molecular weight. The number at the end of the abbreviated polymer names presents the DP of the main chain, e.g. PPG-OH-7 is a hydroxyl terminated PPG consisting of 7 propylene glycol repeat units (i.e. a M_n of 440 g/mol, note that this value contains the MW of the end-groups which is not comprised in the DP).

Synthesis of carboxylic acid terminated polypropylene glycol (PPG-COOH). PPG-NH₂ of $M_n = 480$ g/mol (5.0 g, 12.5 mmol) and triethanolamine (5.23 ml, 37.5 mmol) were dissolved in 40 mL anhydrous tetrahydrofuran (THF). 4- (Dimethylamino) pyridine (1.527 g, 12.5 mmol) and

succinic anhydride (5.0 g, 50 mmol) dissolved in 25 mL anhydrous THF were added to the PPG-NH₂ solution. The reaction (Scheme 1) was performed at 40 °C for 2 days under nitrogen atmosphere. After evaporating the organic solvent, hydrochloric acid solution (40 mL, 1 M) was added, and the mixture was stirred for 1.5 hours. DCM was used to extract the product (30 mL × 4). The organic layer was collected and dried with anhydrous sodium sulfate. Pure product (around 2 g) was obtained after removing the solvent by vacuum. The quantitative end group modification was checked by ¹H NMR (appearance of the characteristic peaks g, h in the succinic acid and the complete downfield shift of peak e after the reaction, Fig. S1).



Scheme 1. (a) Synthesis of carboxylic acid-terminated polypropylene glycol (PPG-COOH) from the amine terminated polypropylene glycol (PPG-NH₂); (b) Synthesis of methyl-terminated polypropylene glycol (PPG-CH₃) from the hydroxyl terminated (PPG-OH).

Synthesis of methyl terminated polypropylene glycol (PPG-CH₃). Methylation of the PPG-OH was performed as follows^{68, 69}: potassium hydroxide (KOH, 0.76 g, 13.6 mmol) was grinded into fine powder and dried in the vacuum oven before use. In a glove box, PPG-OH-7 (1.0 g, 2.27 mmol) was diluted with ethylene glycol dimethyl ether (12 mL). The KOH powder was slowly added into the PPG-OH solution while stirring until totally dissolved. Dimethyl sulfate (0.86 g, 6.81 mmol)

was added to the mixture dropwise. The reaction was performed at room temperature for 2 weeks. The product mixture was transferred to the fume hood to evaporate the solvent (due to the toxicity of reagents). After the majority of the solvent was gone, hexane was added to wash the PPG-CH₃. The resulting polymer was dried under vacuum at room temperature for 3 days. ¹H NMR confirmed the complete methylation of the OH groups (complete shift of peak e which corresponds to the CH group adjacent to the terminal hydroxyl groups in the PPG-OH, Fig. S2).

The results of the telechelic PPG were compared to our earlier data for telechelic PDMS with the same set of chain ends^{66, 67}. Hydride-terminated polydimethylsiloxane (PDMS-H) with labeled MW of 4000-5000 g/mol and hydroxyl-terminated PDMS (PDMS-OH) with labeled MW of 4200 g/mol were provided by Gelest. PDMS-H is denoted as PDMS-H-49 based on ¹H NMR analysis. The M_n of PDMS-OH was characterized by polystyrene (PS) standard GPC as 5600 g/mol, with $DP = 75$ accordingly. Amine-terminated PDMS (PDMS-NH₂) with labeled MW of 900-1000, 3000, 5000 g/mol were purchased from Gelest and denoted as PDMS-NH₂-22, 50 and 74 based on ¹H NMR analysis⁶⁷. Carboxylic acid-terminated PDMS (PDMS-COOH), which have the same end group with PPG-COOH in this work, were synthesized from PDMS-NH₂ with the same DP accordingly. Synthesis details can be found in our previous work⁶⁷.

2.2 Methods. *Differential Scanning Calorimetry (DSC)* measurements were performed using a Q-1000 differential scanning calorimeter (TA Instruments). Samples were dried in a vacuum oven for several days before each measurement to remove any remaining solvents and moisture. In all measurements, the samples were sealed in aluminum hermetic pans and went through the same temperature range of 150 – 350 K at a scan rate of 10 K/min. The cooling and heating cycles were repeated twice to confirm the reproducibility of the results. The glass transition

temperature (T_g) was determined from the midpoint of the heat flow step during the 2nd heating via the TA Universal Analysis 2000 software.

Broadband Dielectric Spectroscopy (BDS) measurements in the frequency range $10^{-2} - 10^7$ Hz were carried out using a Novocontrol Concept-80 system with an Alpha-A impedance analyzer and a Quatro Cryosystem temperature controller. Prior to the measurement, the samples were dried in the same way as described in the DSC protocol. The PPG-OH, PPG-COOH and PPG-NH₂ samples were placed in a parallel-plate dielectric cell made of sapphire and invar steel, similar to the one described in ref⁷⁰. The empty cell, with an electrode diameter of 12 mm and electrode separation of 49 μ m, had a capacitance of 20 pF. The PPG-CH₃ samples were placed between two gold-plated electrodes with a diameter of 10 mm separated by a Teflon spacer of 50 μ m thickness. The experiments proceeded from high to low temperatures. The samples were stabilized at each temperature within 0.2 K for at least 10 min to achieve a thermal equilibrium before each sweep.

Shear rheology. Prior to all rheological measurement the samples were dried in the same way as described above. Small-amplitude oscillatory shear (SAOS) measurements were performed with a stress-controlled mode of the AR2000ex (TA Instruments) in an angular frequency range $10^{-1} - 10^2$ rad/s using parallel plate geometry, with a disk diameter of 4 mm and 8 mm according to the magnitude of the shear modulus. The gap between plates was about 0.5 mm and kept constant for all the investigated temperatures. A strain sweep measurement was performed at each temperature to ensure that the SAOS response was within the linear regime. Before each rheological measurement, a thermal stabilization of 10 minutes was performed to assure thermal equilibrium. Temperature was stabilized within 0.2 K for all measurements. Zero shear viscosity measurements for the $\eta_0 < 10^5$ Pa*s (temperature range from 220 K to 300 K) were conducted

using the same AR2000ex rheometer in continuous ramp measurements with a shear rate of 10 s^{-1} . We used a conical plate of 25 mm in diameter with a cone angle of 2° and a truncation of 58 μm . Zero shear viscosity $\eta_0 > 10^5 \text{ Pa}\cdot\text{s}$ ($T < 220 \text{ K}$) were estimated using terminal relaxation mode in SAOS measurement $\eta_0 = \lim_{\omega \rightarrow 0} G''/\omega$.

3. Results

3.1 Differential scanning calorimetry

The heat flow data for all studied PPG samples exhibit a clear endothermic step (Fig. S3) associated with their glass transition (Table 1). For PPG-CH₃, T_g decreases with decrease of MW, following the normal trend for polymers⁷¹ (Fig. 1a). In case of PPG-NH₂ and PPG-OH, T_g is almost independent of MW with only a slight reduction for small MW, as has been found by other researchers for PPG-OH before⁷². In contrast, T_g of PPG-COOH increases strongly with decrease in MW. The observed behavior of T_g is consistent with known increase in the glass transition temperature of linear associating polymers with intermolecular H-bonds.^{12, 14, 66, 67, 73} Stronger H-bond strength significantly alters the MW dependence of T_g at low molecular weights⁷².

These results (Fig. 1a) are in strong contrast to earlier studies of telechelic PDMS with the same set of chain ends, where no influence of chain end association strength on T_g has been found⁶⁷ (Fig 1b). We emphasize that special care was taken to avoid influence of crystallization on measured T_g in the case of telechelic PDMS studies (for details see ref⁶⁷).

Table 1. Material properties of the investigated polymers: molecular weight MW^* , glass transition temperature as determined by DSC and BDS $T_{g, cal}$, $T_{g, diel}$, respectively.

Sample	DP	M_n [g/mol]	$T_{g, cal}$ [K]	$T_{g, diel}$ [K]
PPG-NH ₂ -6	6	480 ^a	193.7	192.3
PPG-NH ₂ -33	33	2046 ^a	197.4	198.8
PPG-NH ₂ -67	67	4018 ^a	198.5	200
PPG-COOH-6	6	680 ^b	245.5	248.8
PPG-COOH-33	33	2246 ^b	212.6	213.6
PPG-COOH-67	67	4218 ^b	206.1	205.3
PPG-OH-7	7	440 ^b	195.7	196.8
PPG-OH-14	14	846 ^b	197.5	198.8
PPG-OH-18	18	1078 ^b	197.6	200.1
PPG-OH-37	37	2180 ^b	199.1	200.8
PPG-OH-56	56	3282 ^b	198.9	200.8
PPG-CH ₃ -7	7	468 ^c	171.8	172.9
PPG-CH ₃ -14	14	874 ^c	183.1	182.5
PPG-CH ₃ -18	18	1106 ^c	185.7	186.7
PPG-CH ₃ -37	37	2208 ^c	194.3	193.3
PPG-CH ₃ -56	56	3310 ^c	194.2	195.4

^a determined from H1 NMR measurements of PPG-COOH corrected for the end-group exchange

^b determined from H1 NMR measurements

^c determined from H1 NMR measurements of PPG-OH corrected for the end-group exchange

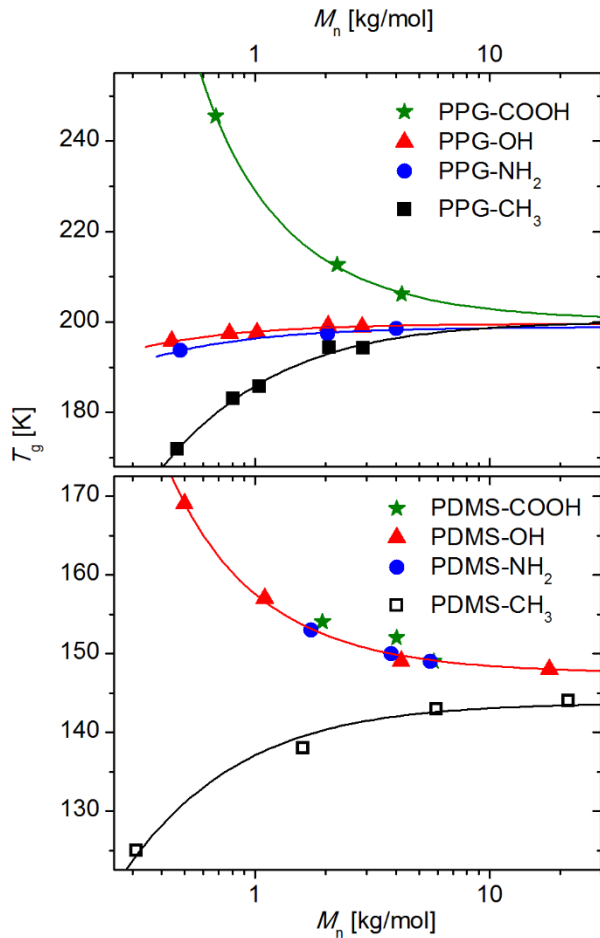


Figure 1. Calorimetric T_g (solid symbols) vs total molecular weight M_n (including end groups) in telechelic PPG (a) and PDMS^{66, 67} (b) with different end-groups, as indicated. The PDMS-CH₃ data are dielectric T_g values taken from ref⁷⁴. The lines are fits to the Fox-Flory equation⁷⁵.

3.2 Dielectric spectroscopy

The dielectric loss spectra of regular PPG show two relaxation processes which is characteristic for type-A⁷⁶⁻⁷⁸ polymers: i) the dielectric α -relaxation at high frequencies that represents segmental relaxation, and ii) the normal mode at lower frequency that represents the end-to-end relaxation (chain modes). The loss spectra of PPG-CH₃-7, PPG-NH₂-6, PPG-OH-7, PPG-COOH-

6, PPG-OH-14 and PPG-CH₃-14 exhibit only one process, while the spectra of all other samples exhibit two relaxation peaks (Fig. 2). The dielectric loss spectra of PPG-OH and PPG-CH₃ are basically similar to those of PPG-NH₂ (all are presented in Fig. S4) and are consistent with literature reports ^{45, 46, 48, 52, 54, 72, 76, 79-84}.

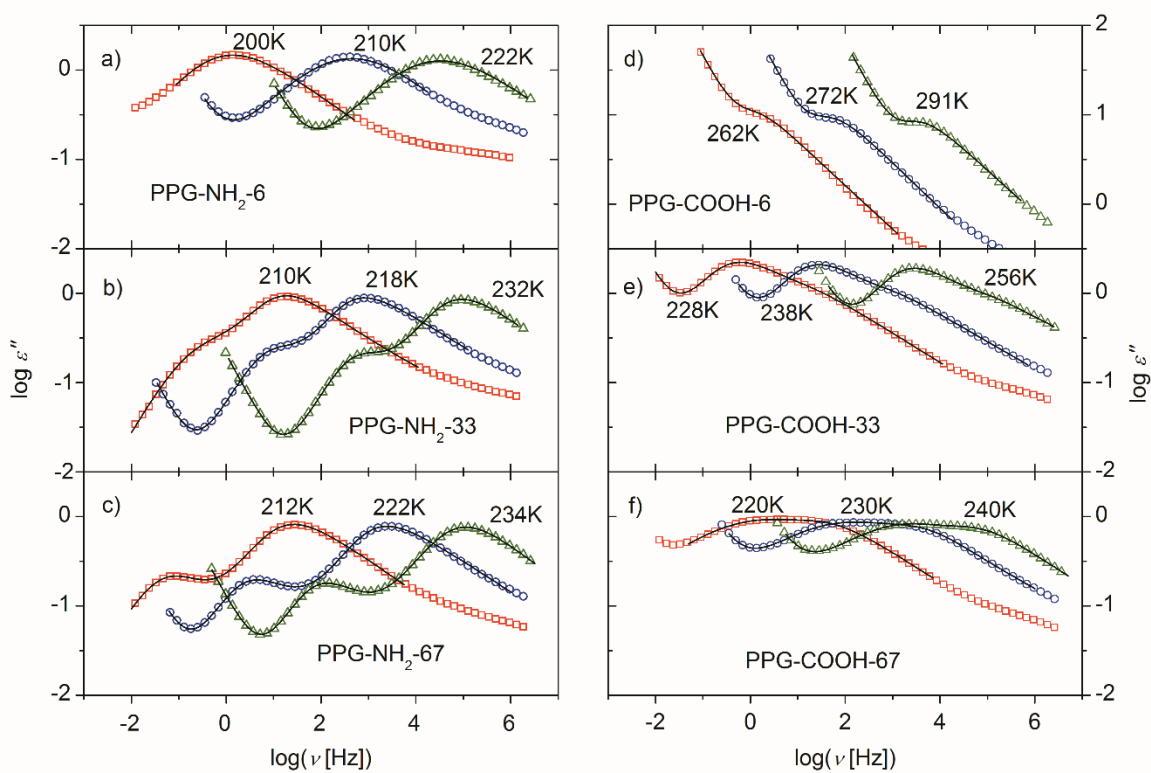


Figure 2. Dielectric loss spectra $\epsilon''(\nu)$ (symbols) at several temperatures as indicated of PPG-NH₂ with DP of 6 (a), 33 (b) and 67 (c) and PPG-COOH with DP of 6 (d), 33 (e) and 67 (f). The solid lines are fits to functions consisting of one/two HN functions and a conductivity contribution (eq. 1).

The spectra of PPG-COOH-33 and PPG-COOH-67 also show two relaxation processes (Fig. 2e and 2f), but these are much closer in frequency than in the other systems with similar MW (see e.g. Fig. 2b and 2c). Moreover, the normal mode amplitude is lower than the segmental peak amplitude in the spectra of CH₃-, OH- and NH₂-terminated PPG, while in the spectra of the COOH- terminated PPG the lower frequency peak is stronger, and the higher frequency peak appears as a shoulder. To analyze the spectra, we fit them using two Havriliak-Negami (HN) functions (with indices 1 and 2, respectively) and a conductivity contribution:⁷⁶

$$\varepsilon^*(\nu) = \varepsilon_{\infty} + \frac{\Delta\varepsilon_1}{[1 + (i2\pi\nu\tau_1)^{\alpha 1}]^{\gamma 1}} + \frac{\Delta\varepsilon_2}{[1 + (i2\pi\nu\tau_2)^{\alpha 2}]^{\gamma 2}} + \frac{\sigma}{2\pi i \nu \varepsilon_0} \quad (1)$$

Here, ε_{∞} denotes the permittivity in the high frequency limit, $\Delta\varepsilon$ is the relaxation strength, τ is the HN relaxation time, $i = (-1)^{0.5}$ is the imaginary unit, the parameters α and γ describe the shape of the relaxation peak, σ corresponds to the DC conductivity and ε_0 is the permittivity of vacuum. For the fits of the spectra which exhibit only one clear relaxation peak (the low MW samples), the relaxation strength of one of the HN functions is fixed to zero. In the PPG-COOH-33 spectra, the low-frequency process overlaps with the high-frequency peak which appears only as a shoulder, so its low-frequency wing is not visible. Consequently, the respective parameter α describing the slope of this wing is fixed to the value 0.864 (as obtained from the average of α in NH₂-, OH- and CH₃-terminated PPG). The characteristic relaxation time that corresponds to the maximum position of the loss peak (a collection of these relaxation times is given in Tables T1-T4 in the Supplementary Material) can be calculated using the expression⁷⁶:

$$\tau_{\max} = \tau \left[\sin\left(\frac{\alpha\pi}{2+2\gamma}\right) \right]^{-\frac{1}{\alpha}} \left[\sin\left(\frac{\alpha\gamma\pi}{2+2\gamma}\right) \right]^{\frac{1}{\alpha}} \quad (2)$$

The temperature dependence of τ_{\max} is non-Arrhenius and can be fitted by the Vogel-Fulcher-Tamman (VFT)^{76, 85-87} equation in all samples (Fig. 3):

$$\tau_{\max} = \tau_0 \exp\left(\frac{B}{T - T_0}\right) \quad (3)$$

where τ_0 , B , and the so-called VFT temperature T_0 are fitting parameters. From these parameters, also the fragility index m can be calculated:

$$m \equiv \left[\frac{\partial \log_{10} \tau}{\partial (T_g/T)} \right]_{T=T_g} = \frac{BT_{g,diel}}{\ln 10 (T_{g,diel} - T_0)^2} \quad (4)$$

which indicates the steepness of the temperature dependence of the relaxation time at T_g , and is considered to reflect the frustration in molecular packing^{88, 89} (Tab. 2).

Table 2. VFT parameters (eq. 3) and fragility index m of the dielectric relaxations of PPG terminated with different chain ends.

Sample	Fast process				Slow process			
	$\log(\tau_0$ [s])	B [K]	T_0 [K]	m	$\log(\tau_0$ [s])	B [K]	T_0 [K]	m
PPG-NH ₂ -6	-13.2	1128	160	92	-	-	-	-
PPG-NH ₂ -33	-12.7	1002	169	99	-11.4	1383	155	60
PPG-NH ₂ -67	-12.8	1022	170	98	-10.3	1244	162	58
PPG-COOH-6	-	-	-	-	-11.5	1405	204	74
PPG-COOH-33	-12.6	1129	180	93	-11.5	1403	172	65
PPG-COOH-67	-13.9	1303	170	91	-12.6	1473	165	69

PPG-OH-7	-13.1	1270	160	81	-	-	-	-
PPG-OH-14	-13.1	1206	164	87	-	-	-	-
PPG-OH-18	-12.8	1079	168	94	-	-	-	-
PPG-OH-37	-12.7	1052	170	95	-11.8	1554	153	57
PPG-OH-56	-12.7	1044	170	96	-11.5	1500	156	57
PPG-CH₃-7	-13.5	1161	141	83	-	-	-	-
PPG-CH₃-14	-12.6	965	154	93	-	-	-	-
PPG-CH₃-18	-13.0	1045	156	98	-	-	-	-
PPG-CH₃-37	-12.8	1032	163	95	-11.4	1327	153	61
PPG-CH₃-56	-12.1	874	168	102	-10.8	1276	156	59

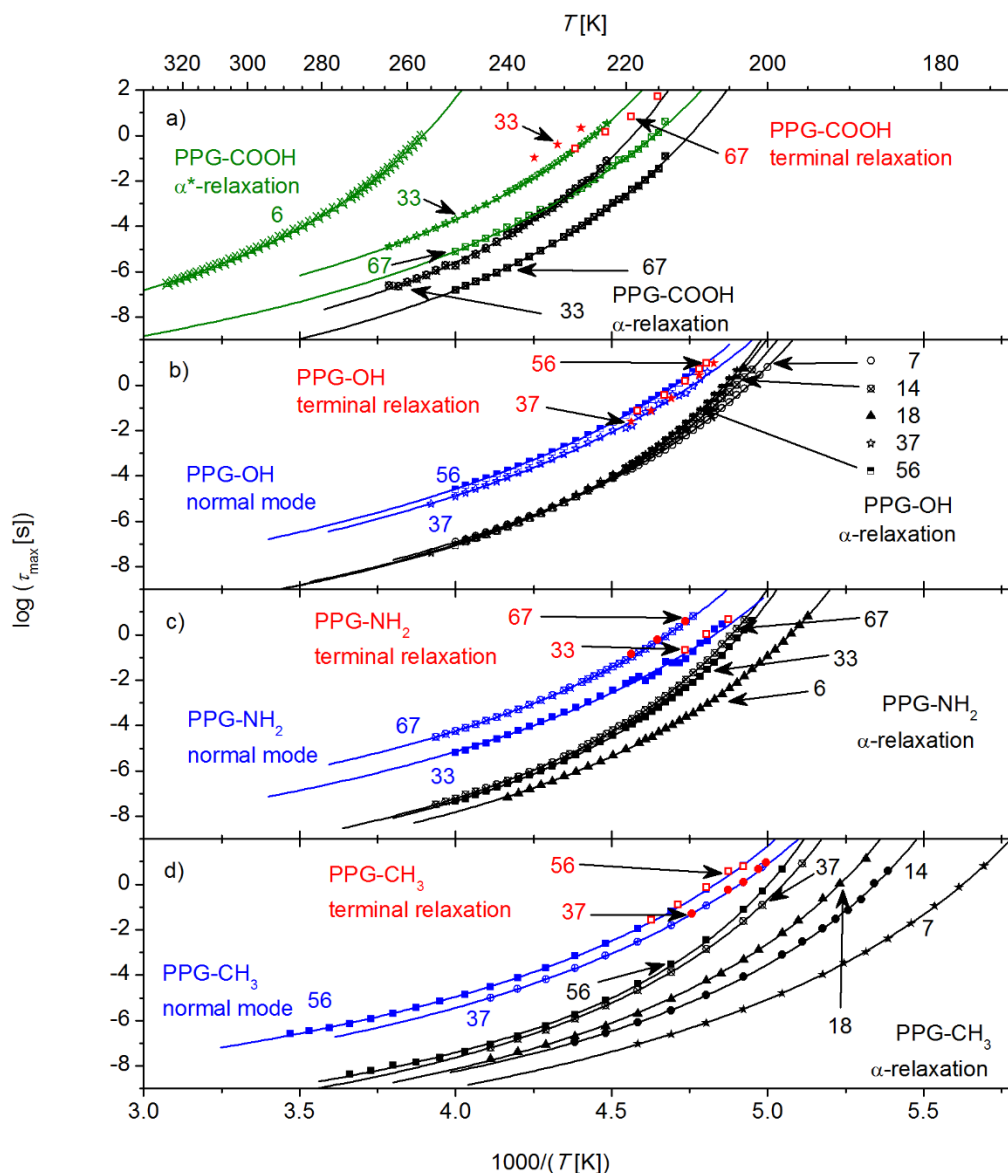


Figure 3. Arrhenius plot of the mean relaxation time of dielectric relaxations for (a) PPG-COOH, (b) PPG-OH, (c) PPG-NH₂ and (d) PPG-CH₃ with different *DP* as indicated by the numbers. The solid lines are fits to the VFT equation (eq. 3). Additionally, the relaxation times of the terminal relaxation as determined from the shear modulus spectra are shown; we note that the rheological segmental relaxation times (not shown for clarity) are significantly slower than the dielectric α -relaxation times.

Since in PPG-COOH spectra the normal mode is not visible (its amplitude is significantly smaller than the segmental peak), we also analyzed the derivative of the real part of the permittivity⁹⁰

$$\varepsilon'_{der} = -\frac{\pi\partial\varepsilon'(\omega)}{2\partial\ln\omega} \quad (5)$$

This representation can help to unravel relaxation processes which are obscured by Ohmic conductivity or adjacent processes in the loss spectra. The derivative spectra of PPG-COOH-67 indeed reveal a third relaxation process which appears as a shoulder at the low-frequency wing of the slower process (Fig. 4). In order to extract its characteristic relaxation time, we fitted the data to a Havriliak-Negami function modified for the derivative representation (see ref⁹⁰).

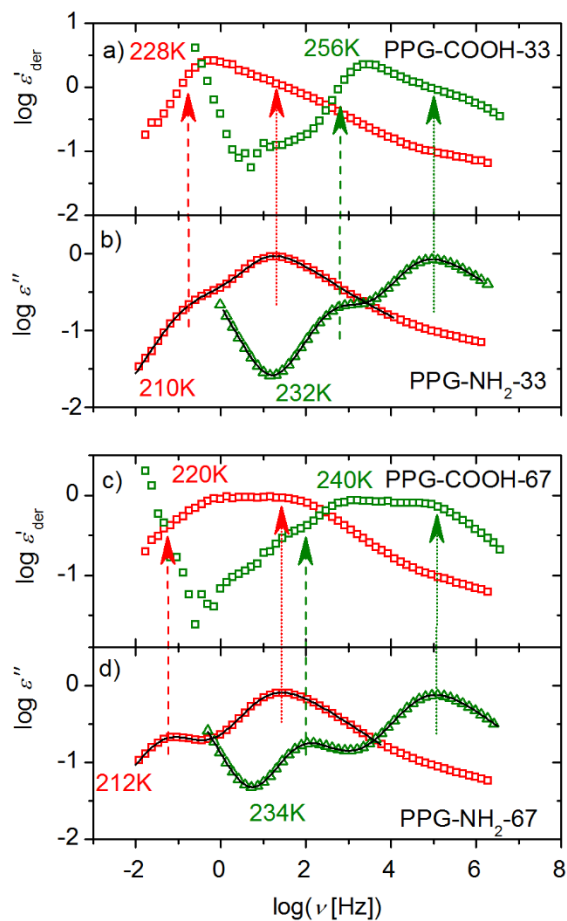


Figure 4. a) and c) Spectra of $\varepsilon'_{\text{der}}$ of PPG-COOH with DP of 33 and 67, respectively, at several temperatures as indicated, as well as b) and d) the dielectric loss spectra ε'' of the corresponding PPG-NH₂. The temperatures of the latter were chosen to roughly match the α -relaxation peaks with the PPG-COOH of the same DP in order to compensate the difference in T_g . The solid lines are fits to eq. 1.

3.3 Shear rheology and viscosity

The shear modulus master curves of all measured PPG samples were constructed by horizontal shifting of the shear modulus loss spectra until a best match with the spectra of the respective

previous temperature scan was achieved. Although the underlying assumption of time-temperature superposition (tTS) may not be accurate in our case, the master curves can still provide a general picture of the mechanical properties and unravel distinctive processes of stress relaxation⁶⁷. The shear modulus spectra (examples of telechelic PPG-COOH are presented in Fig. 5) show the typical polymer features: i) at high frequencies, the value G_∞ is found in the GPa range common for segmental dynamics and $G''(\omega)$ exhibits a peak of segmental relaxation; ii) Rouse modes follow at lower frequencies, and iii) terminal relaxation ($G'(\omega) \sim \omega^2$ and $G''(\omega) \sim \omega^1$) appears at lowest frequencies. The separation between segmental relaxation and terminal mode becomes larger with increasing MW. In order to extract the respective timescales, the data sets have been fit to a function composed of a generic peak function⁷⁶ to account for contributions of segmental and chain dynamics:

$$G' = \frac{A}{[(\omega\tau_s)^{b_1} + (\omega\tau_s)^{b_2}]} + G_e \frac{\omega^2\tau_c^2}{1 + \omega^2\tau_c^2} \quad (6a)$$

$$G'' = \frac{A}{[(\omega\tau_s)^{c_1} + (\omega\tau_s)^{c_2}]} + G_e \frac{\omega\tau_c}{1 + \omega^2\tau_c^2} \quad (6b)$$

Where ω is the angular frequency, A and G_e represent the plateau moduli in the glassy and terminal regime, respectively, and τ_s and τ_c are the characteristic relaxation times of the segmental and terminal relaxation, respectively. The parameters b_1 and b_2 as well as c_1 and c_2 are the low and high frequency slopes of the G' and G'' curves, respectively. We note that this is a very rough approximation of the complex rheological spectra, and its generic shape includes the contribution of additional dynamics like Rouse modes which are very difficult to fit separately. Moreover, the first term in G' and G'' does not satisfy Kramers-Kronig relationship which is known to be valid for linear viscoelastic regime. Thus the approximation⁷⁶ is not valid for

rigorous analysis of the relaxation spectra. However, this approximation is sufficient to estimate the characteristic relaxation times of segmental and terminal modes. The obtained relaxation times refer to the reference temperature. However, if the two processes have different temperature dependence, the constructed master curve will suffer from a corresponding distortion. Failure of tTS in our case is reflected in the slight difference in the temperature dependencies of the shift parameter a_T and the dielectric α -relaxation (Fig. 5). To obtain the terminal relaxation times at those temperature where they were actually measured (and not at the reference T) we divided the characteristic relaxation time obtained from the master curve by the shift factor at the respective temperature.

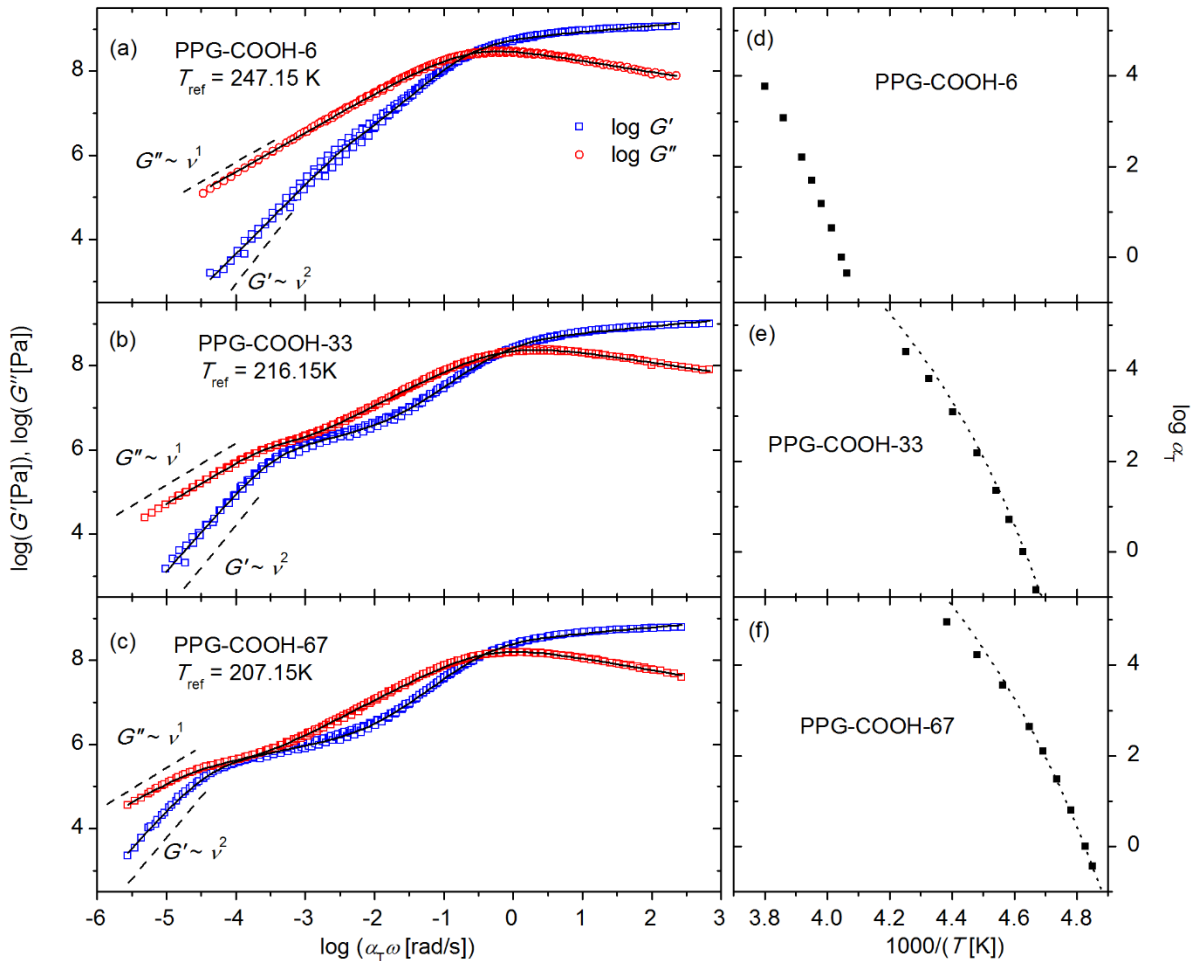


Figure 5. Shear modulus master curves constructed from linear viscoelastic spectra using tTS for PPG-COOH with (a) $DP = 6$, (b) $DP = 33$ and (c) $DP = 67$, and the respective shift parameters (d-f). The solid lines are fits to eq. 4, the dashed lines display the typical slopes in the terminal regime as indicated, and the dotted lines represent the temperature dependence of the dielectric α -relaxation time.

Normalized shear modulus master curves $G'(\nu/\nu_{\max})/G_{\infty}$ and $G''(\nu/\nu_{\max})/G''_{\max}$ (here G_{∞} is the high frequency plateau value of G' , and G''_{\max} and ν_{\max} represent the glassy relaxation peak maximum and position in G'') of PPG with similar molecular weight clearly reveal the impact of the different end groups (Fig. 6). The terminal relaxation for all OH-, NH₂- and COOH-terminated PPG shifts to lower frequencies in comparison to that of non-associating PPG-CH₃. The separation between the loss maximum and the onset of (an apparent) terminal mode becomes significantly larger for PPG-COOH. Since similar molecular weights are compared, this shift in terminal relaxation must be a consequence of the chain end association.

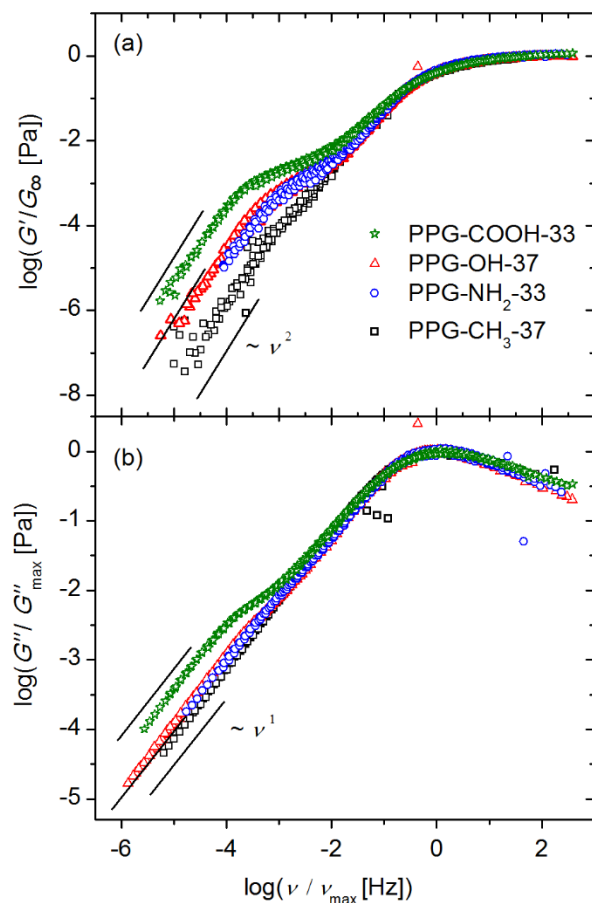


Figure 6. Storage (a) and loss part (b) of the shear modulus master curves normalized with respect to the respective maxima $G'(\nu/\nu_{\max})/G_{\infty}$ and $G''(\nu/\nu_{\max})/G''_{\max}$ as well as the frequency position ν_{\max} of G''_{\max} obtained using tTS for PPG of different end-groups as indicated and similar DP . The dashed lines indicate the terminal end of the spectra.

To compensate for the impact of the difference in segmental dynamics, we present the zero shear viscosity of different telechelic PPG vs T_g -scaled temperature (Fig. 7). The viscosities vs T_g/T for the NH₂ and OH terminated PPG differ only slightly from the viscosity of the CH₃ terminated system, while the viscosity increases by almost one decade for the COOH-terminated PPG. A

similar analysis of the viscosity has been performed for telechelic PDMS with the same set of chain ends⁶⁷. In that case, a significant alteration in the viscosity, even after scaling out the role of T_g , was found for COOH terminated chains, while only a weak effect was observed for OH and NH_2 terminated PDMS (Fig. 7b).

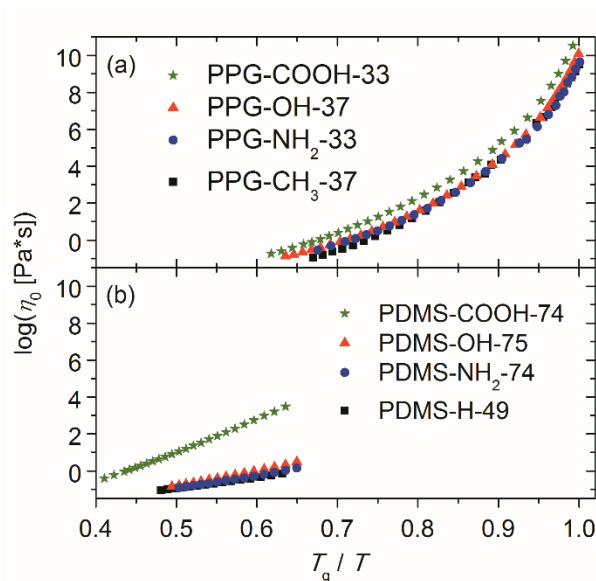


Figure 7. Zero shear viscosity η_0 vs T_g/T for telechelic PPG (a) and PDMS (from continuous ramp measurements⁹¹) (b) with different end-groups as indicated with DP of 33-37 and 75, respectively.

4. Discussion

4.1 Impact of associating end-groups on T_g

One peculiar observation is the very different dependence of T_g (segmental dynamics) and viscosity (chain dynamics) on the strength of H-bonding end-groups association in the PPG systems. T_g increases significantly with increasing interaction strength, especially at lower MW

(Fig. 1a). However, once the shift in T_g is accounted for (by scaling the temperature by T_g), the viscosity shows only a very small increase with increase in strength of the chain end interaction strength (Fig. 7a). This means, that beyond the increase of T_g , viscosity does not undergo any significant enhancement. This result strongly contrasts our previous findings in telechelic PDMS terminated with the same end-groups^{66, 67}. In this more flexible backbone, the increase in T_g is similar for all three H-bonding end-groups independent of the interaction strength (Fig. 1b). However, the T_g -scaled viscosity of PDMS-COOH is enhanced by about 2-3 orders of magnitude compared to the chains with weaker or non-H-bonding end-groups (Fig. 7b). These trends suggest that the difference in the backbone flexibility might play a significant role for the consequences chain-end association has on the system properties. We would like to note that larger effects seen in COOH terminated PDMS chains compared to the other two H-bonding systems may be due to the additional amide group⁶⁷. In similar systems, urea and urethane groups were found to establish additional lateral H-bonds reinforcing the supramolecular structure⁹². Moreover, this end group seems to have the tendency to phase separate in PDMS, as evidenced from two T_g 's observed in DSC data of PDMS-COOH systems⁶⁷.

The most surprising result is that T_g in the telechelic PDMS is essentially independent of the H-bond strength, while it changes strongly for telechelic PPG with different end-groups (Fig. 1). We speculate that the chain end association in telechelic PDMS even in the weaker OH and NH₂ terminated chains essentially freezes the motions of the chain end segments at temperatures below ~ 180 K. In a simple picture, the end-groups and the adjacent segments may be considered as the high- T_g component of a miscible polymer blend or a co-polymer. An increase in molecular weight leads to a decrease of the volume fraction of this high- T_g component, and the measured T_g approaches the T_g of non-associating chains (Fig. 1). However, at higher temperatures, e.g. T_g of

PPG $\sim 200\text{K}$, the structural relaxation of the chain ends of OH and NH_2 terminated PPG becomes comparable to the segmental relaxation of long PPG chains. This would result in an essentially molecular weight independent T_g (Fig. 1a). In contrast, the stronger COOH association still freezes the PPG end segments even at $T \sim 250\text{K}$. This leads to the significant increase in T_g with decrease in MW for COOH- terminated PPG (Fig. 1a). Thus, the main difference in the behavior of segmental dynamics in these telechelic PDMS and telechelic PPG is the temperature range defined by their backbone flexibility. The much lower T_g of PDMS ($\sim 145\text{K}$) makes even weaker H-bonding end-groups (e.g. NH_2 and OH) form strong enough associations which slow down the chain-ends and adjacent segments significantly. In contrast, at the higher T_g of PPG ($\sim 200\text{K}$) these associations are weaker, resulting in structural relaxation times of the end segments with OH and NH_2 groups which are comparable to the segmental dynamics of the main chain. Only the end segments with COOH groups remain significantly slower leading to an increase of the overall T_g with decrease in MW.

4.2 Assignment of dielectric relaxations.

For all the samples exhibiting two dielectric relaxations, the extrapolation of the VFT fits of the faster process to a mean relaxation time of 100 s yields a temperature that agrees well with the calorimetric $T_{g,\text{cal}}$ (Table 1). Consequently, we can identify the high-frequency process with the dielectric alpha-relaxation (segmental mode) and refer to the extrapolated temperature as the dielectric glass transition temperature $T_{g,\text{diel}}$. Also, the rather large fragility index m of this process (Tab. 2) is indicative for segmental relaxation. These characteristics hold also for the single relaxation observed in PPG-CH3-7, PPG- NH_2 -6 and PPG-OH-7, and thus this process can also be assigned to the segmental relaxation. Only for the PPG-COOH-6, $T_{g,\text{diel}}$ is more than 3K

higher than $T_{g,cal}$, and the respective process has a much lower fragility index (Tab. 2); a point which will be discussed below.

The separation of the slower relaxation peak from the segmental peak in the spectra of CH₃, NH₂ and OH terminated samples decreases with decreasing MW, as is expected for the normal mode.⁷⁶ There is no normal mode in the spectra of the smallest *DP* (~7 repeat units). Good agreement between the relaxation time of the slow dielectric mode and of the terminal relaxation time (Fig. 3) supports the assignment of the slow dielectric process in CH₃, NH₂ and OH terminated PPG to the normal mode.

In contrast, the slower process in the loss spectra of COOH terminated PPG exhibits approximately the same separation from the segmental relaxation, in all molecular weights where the two can be separated (Fig. 3a). Furthermore, its relaxation strength by far exceeds that of the normal mode observed in other PPG samples of similar MW, and it grows drastically with decreasing MW (Fig. 8). In fact, the relaxation strength of this process exhibits linear dependence on inverse *DP* (inset Fig. 8). Finally, in the derivative spectra of the permittivity of PPG-COOH-67 the normal mode relaxation can be observed precisely where it is expected based on the PPG-NH₂-67 data (Fig. 4). All these observations suggest that the slower process in the dielectric loss spectra of COOH terminated PPG is not the chain mode; instead, it reflects apparently a phenomenon which happens at the chain ends. Since it follows a VFT-like temperature dependence that is roughly parallel to the segmental relaxation with a separation of ~2 decades, a relation between these two processes can be assumed. Most likely, the slower process is related to the chain-end association/dissociation, as has been found in several other H-bonding supramolecular polymers^{15, 67, 93-95}, and we refer to it as the α^* -relaxation. We assume that in PPG-COOH-6, the α^* -relaxation dominates the spectra and the segmental relaxation is

hidden in its high frequency wing. This explains the largest difference between $T_{g, \text{diel}}$ and $T_{g, \text{cal}}$ observed for this sample (Table 1).

The α^* -relaxations have been also observed in our earlier studies of NH_2 terminated telechelic PDMS⁶⁷ at frequencies lower than the segmental relaxation. However, in the cases of PPG- NH_2 and PPG-OH no such contribution is visible; the only process present in the low frequency region of the spectra is plausibly identified as the normal mode (Fig. 9). Our previous results on PDMS suggest that the dielectric relaxation strength of the α^* -process of these end-groups is significantly lower than $\epsilon''(\omega) < 0.1$ ⁶⁷, and is too weak to be detectable in the PPG samples where the low frequency range is dominated by their normal mode relaxations with the amplitude $\epsilon''(\omega) > 0.2$ (Fig. 9).

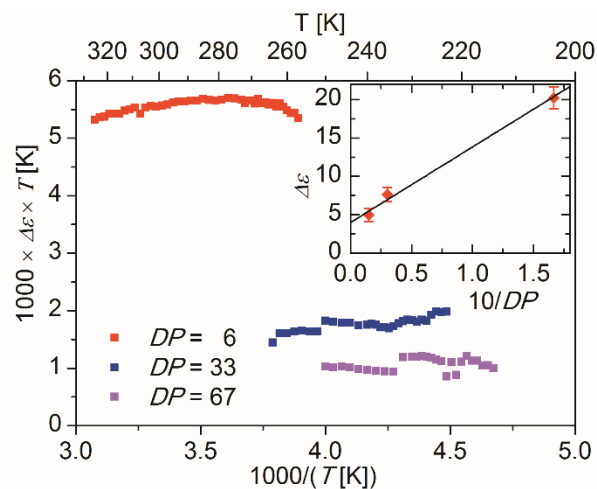


Figure 8. Temperature dependence of the product of dielectric relaxation strength with temperature $\Delta\epsilon T$ of the slower process of PPG-COOH with DP as indicated. Inset: dependence of the dielectric relaxation strengths of the slower process of PPG-COOH on the inverse of DP . The amplitudes of the peaks were averaged over several temperatures in the range where the

peaks are well within the measured spectral window (266 – 297 K for PPG-COOH-6, 225 – 248 K for PPG-COOH-33 and 214 – 232 K for PPG-COOH-67).

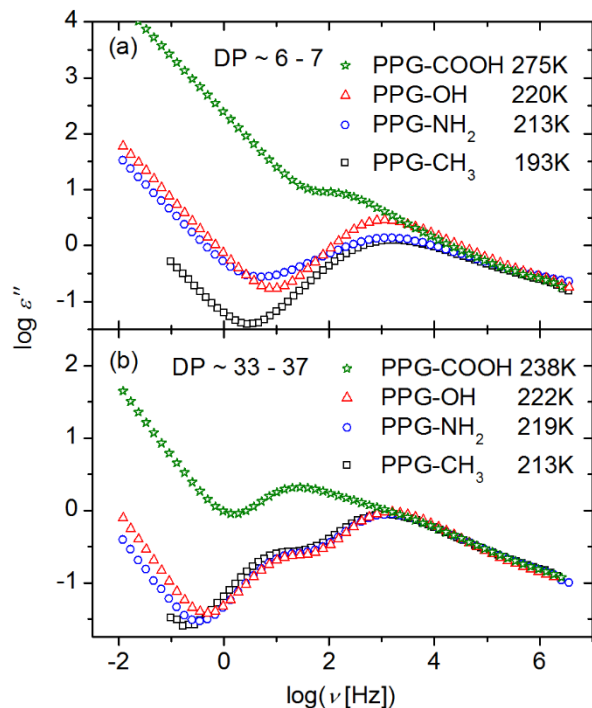


Figure 9. Dielectric loss spectra $\epsilon''(\nu)$ of PPG with different end-groups as indicated and DP of (a) 6-7 and (b) 33-35. Note that the curves are not normalized; to account for the change in T_g , different temperatures were chosen as indicated to match the α -relaxations.

4.3 Activation energies of the chain-end association.

To estimate the characteristic chain-end dissociation energy E_a , we follow the recently proposed consideration that the segmental dynamics defines the attempting dissociation rate, and E_a can be obtained from the difference in relaxation time between the α - and the α^* -relaxation:^{44, 93-95}

$$\tau_{\alpha^*}(T) = \tau_{\alpha}(T) \exp\left(\frac{E_a}{RT}\right) \quad (7)$$

Where R is the universal gas constant. Using the VFT fit parameters of the respective α -relaxation to fix $\tau_{\alpha}(T)$, and keeping E_a as the only free parameter in the eq. 7, we estimated the activation energies of the α^* -relaxation to be $8.5 (\pm 0.1) \text{ kJ mol}^{-1}$ and $7.2 (\pm 0.1) \text{ kJ mol}^{-1}$ for PPG-COOH with DP of 33 and 67, respectively (Fig. 10). For the single process observed in the dielectric spectra of PPG-COOH-6 we have several indications that it is the same chain-end dissociation process: its estimated T_g is significantly higher than that obtained from DSC, meaning that it seems to be slower than the α -relaxation. Also its fragility index m is close to that of the α^* -relaxations (Tab. 2). Based on this assignment, we can estimate $\tau_{\alpha}(T)$ in this sample using eq. 7 and assuming an activation energy of 8 kJ/mol. The obtained temperature dependence of the segmental relaxation is presented as the dashed-dotted line in the Fig. 10, and its extrapolation to $\tau_{\alpha} = 100 \text{ s}$ provides an estimate of $T_{g, \text{diel}}$ somewhat closer to the calorimetric T_g , which further supports our assignment of the major process (Fig. 3a) to the chain-end dissociation process.

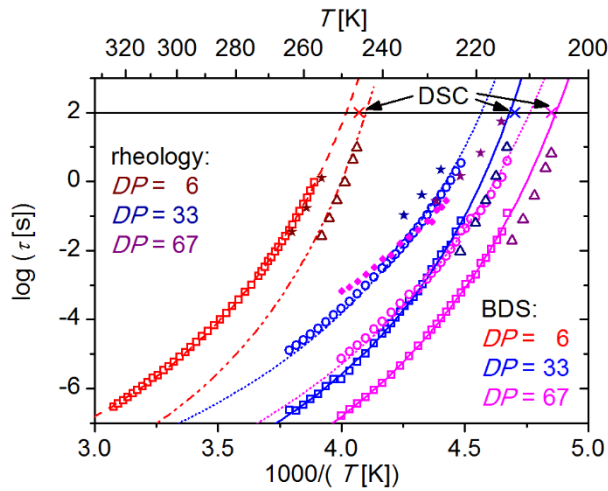


Figure 10. Arrhenius plot of the dielectric mean relaxation time of the α -relaxation (open squares) and the α^* -relaxation (open circles) obtained from the ϵ'' spectra, as well as the normal mode (solid diamonds) obtained from the ϵ'_{der} spectra, the calorimetric T_g (crosses), and the rheological segmental relaxation (open triangles) and terminal relaxation (solid stars) for PPG-COOH with different DP as indicated. The solid and dashed lines are VFT fits, and the dotted lines are fits to eq. 5 where the VFT parameters were fixed to the values obtained for the α -relaxation (see text for details). The dash-dotted line represents the estimated temperature dependence of the α -relaxation in PPG-COOH-6 sample, assuming $E_a = 8$ kJ/mol and that the dielectric relaxation process presents the chain-end dissociation.

We want to emphasize that the estimated values of the COOH dissociation energy is much smaller than the dissociation energies reported for carboxylic acid terminated polyisoprene in solution (~ 100 - 130 kJ/mol⁶), and for COOH-terminated PDMS melts in our previous work (~ 85 - 120 kJ/mol⁶⁷). The difference is that in these two cases the apparent activation energy (the slope in the Arrhenius plot) was identified as the dissociation energy. This is not correct, however, because the temperature dependence of the dissociation process is additionally affected by the temperature dependence of segmental relaxation (eq. 7). We emphasize that authors of Ref⁶ actually discussed that the estimated activation energy is affected by two factors, segmental mobility and by re-association of dissociated chain ends. The latter emphasizes that the mechanical relaxation time does not reflect the dissociation time (see the discussion below), while former essentially agrees with the eq.7. Thus, one needs to take the temperature dependence of segmental dynamics explicitly into account for accurate estimates of the dissociation energy barrier specifically imposed by the H-bonds. Additionally, the polarity of the

medium where the dissociation of chain ends occurs might play a role. In the case of PPG, the dissociation energy for H-bonding end groups might be significantly smaller than in PDMS, because these groups will have some attractive interactions with hydrophilic PPG, but not with hydrophobic PDMS.

Since in the shear modulus master curves we observed a trend of increasing separation between segmental and terminal relaxation with increasing association strength of the end-group (Fig. 6), one might be inclined to presume the same mechanism behind the prolonged terminal relaxation and the α^* -relaxation from the dielectric spectra. However, the analysis of the characteristic times of these two processes (Fig. 10) reveals, that in PPG-COOH of DP 33 and 67 the separation between the rheological terminal and segmental relaxations is significantly larger than between the dielectric α^* - and α -relaxations. This difference originates from the fact that these two processes seem to reflect different molecular mechanisms in the chain end dissociation^{44, 93-95}. The dielectric relaxation represents the rate of the chain end dissociation since this process involves a change in a dipole moment, which happens every time the chain ends associate or dissociate. In contrast, the process in shear modulus reflects a macroscopic stress relaxation which requires a switch of the associated chain-end from one partner chain to another⁹³⁻⁹⁵. Dissociation and reassociation with the same bond partner will not provide stress relaxation, but will appear in the dielectric spectra. It means that mechanical relaxation probes the rate of partner exchange which depends not only on the dissociation rate, but also on the probability to find another associating chain-end relative to the probability to reconnect to the same initial chain-end. It has been proposed⁹³⁻⁹⁵ that the rheologically detectable timescale τ_r comprises a certain number n of dissociation and reassociation events with the same partner, and additionally the time of chain end diffusion, before a new partner can be reached. Thus, the mechanical

relaxation does not provide direct estimates of the dissociation energy. At that point we will not go deeper into an analysis of these results because it requires relatively long discussion and complex data analysis, and this is not the major focus of the current manuscript.

4.4 Interplay of end-group association, segmental dynamics and shear viscosity.

The above discussion demonstrates the complex interrelation of segmental dynamics, chain dynamics and the end-group association. Segmental dynamics is affected by any associating end-groups as reflected by the increase in T_g compared to non-associating reference systems. This increase is large for short chains and diminishes with increasing MW (Fig. 1). For strong associations there seems to be a limit in the T_g increase while intermediate interaction strengths can yield, depending on their dissociation energy, any T_g shift between this limit and the behavior of the reference. Additionally, the strength of the chain-end association depends on temperature; the same OH and NH₂ end-groups provide strong association for PDMS at its characteristic $T_g \sim 145$, while they have only intermediate association strength in PPG with $T_g \sim 200$ K (Fig. 1). Consequently, the chain flexibility strongly affects the chain-end association simply through the relationship of the association energy to T_g that controls the characteristic chain-end dissociation time.

Furthermore, we suspect that the possibility of the end-groups to form H-bonds with the PPG backbone additionally reduces the energy barrier for dissociation of H-bonding end groups in this polymer. Thus, we expect that the dissociation time of the H-bonding chain-ends is additionally reduced in PPG relative to the case of PDMS. In fact, PDMS-COOH exhibits a

larger separation of α^* - and α -relaxation than PPG-COOH which supports the view that apparently the polarity of the surrounding medium is important as well.

A different relation to the end-group association is found for the macroscopic mechanical properties, e.g. terminal relaxation and viscosity, because these are governed primarily by the relaxation of the whole chain. Several timescales are involved: i) the local dissociation time, governed by the segmental relaxation time and activation energy of dissociation (eq. 5); ii) the time it takes a chain-end to switch its association partner (i.e. partner-exchange time), defined by the probability for the dissociated chain end to find another chain, which should vary strongly with MW; and iii) the longest relaxation time of a similar chain without association (i.e. normal chain relaxation). If the partner-exchange time is of the same order or longer than the normal chain relaxation, both zero shear viscosity and terminal relaxation time will increase compared to the reference system with non-H-bonding end-groups (even after scaling out the effect of T_g). However, if the normal chain relaxation time is much longer than the partner-exchange time, the terminal relaxation time and viscosity will be defined by this normal chain relaxation time, i.e. these will be similar to the behavior of non-associating chains.

In particular, the partner-exchange time in the PDMS based systems apparently exceeds the normal chain relaxation only in case of COOH end-groups, while for OH and NH₂ chain-ends it is shorter than the chain relaxation time, resulting in the strong increase of viscosity in the former and no significant change in the latter two (Fig. 7b). In contrast, in the PPG based systems the temperature is higher (larger T_g) and the matrix is more polar, both of which result in weaker associations for the same end-groups. As a result, even in the case of PPG-COOH the dissociation time appears to be significantly shorter than the chain relaxation time (Fig. 10). This leads to the partner-exchange time also being shorter than or comparable to the normal chain

relaxation time in PPG. This explains similar behavior of viscosity (scaled by T_g) in all PPG samples regardless of their chain-ends (Fig. 7a).

In more general terms, for the design of materials with enhanced mechanical properties based on associating functional groups, just considering the activation energy for dissociation of those groups is insufficient. Instead, the ratio of dissociation time to the segmental and chain relaxation times as well as the probability to find a new partner available for association (i.e. chain length) must be taken into account.

5. Conclusion

We studied the impact of H-bonding interaction strength and molecular weight in telechelic PPG using DSC, dielectric spectroscopy and linear rheology. As expected, the chain-end interactions lead to a slowdown of segmental dynamics, an increase in T_g , and both effects are larger for smaller MW. However, the magnitude of this increase in PPG strongly depends on the chain-end interaction strength. This is in contrast to our previous results on telechelic PDMS where the T_g shift was essentially independent of the strength of the chain-end H-bonding⁶⁶. At the same time, zero shear viscosity corrected for the shift in T_g is almost independent of the type of end-group in telechelic PPG, while large differences were found in telechelic PDMS with the same set of end-groups. We explain these observations by the differences in chain-end dissociation time relative to the timescale of the respective structural motion (faster segmental relaxation – T_g vs slower chain relaxation – viscosity). In telechelic PPG, these chain-end dissociation times, as measured by dielectric spectroscopy, do not exceed the normal chain relaxation even for the end-group with the strongest interactions studied here (COOH). Consequently, viscosity is barely affected

in strong contrast to the case of PDMS in our previous study where the viscosity of the COOH-terminated chains exhibits a pronounced increase. In this system, the dissociation of the end-groups is much slower, partially due to the lower temperature at which the relaxations take place in this material.

We would like to emphasize that the segmental relaxation rate plays a fundamental role in defining the timescale of the dissociation process. This means that the activation energy of the functional groups alone is not sufficient to describe their impact on the macroscopic mechanical properties. Instead, we should consider the rate of dissociation which is based on both the segmental relaxation and activation energy for dissociation. Furthermore, to realize a mechanical relaxation of the system, also the probability for a dissociated-chain end to switch from its current partner to another one must be considered. Comparing this partner exchange rate with the chain relaxation rate eventually allows predictions for the resulting macroscopic viscoelastic properties. In other words, the associating groups must be selected particularly for a specific polymer to ensure that, in combination with segmental relaxation and partner exchange probability, the chain relaxation can be matched accordingly to achieve the desired properties.

Acknowledgments: This work was supported by the NSF Polymer program under grant DMR-1408811. MT is grateful to the Alexander von Humboldt Foundation for granting him a Feodor-Lynen fellowship. PC and TS acknowledge partial financial support for polymer synthesis by the U.S. Department of Energy, Office of Science, Basic Energy Sciences, Materials Science & Engineering Division.

Reference

1. Brunsveld, L.; Folmer, B. J. B.; Meijer, E. W.; Sijbesma, R. P. Supramolecular Polymers. *Chem. Rev.* **2001**, *101*, 4071-4097.
2. De Greef, T. F. A.; Smulders, M. M.; Wolffs, M.; Schenning, A. P. H. J.; Sijbesma, R. P.; Meijer, E. W. Supramolecular Polymerization. *Chem. Rev.* **2009**, *109*, 5687-5754.
3. Yang, L.; Tan, X.; Wang, Z.; Zhang, X. Supramolecular Polymers: Historical Development, Preparation, Characterization, and Functions. *Chem. Rev.* **2015**, *115*, (15), 7196-239.
4. Pollino, J. M.; Weck, M. Non-covalent side-chain polymers: design principles, functionalization strategies, and perspectives. *Chem. Soc. Rev.* **2005**, *34*, (3), 193-207.
5. Seiffert, S.; Sprakel, J. Physical chemistry of supramolecular polymer networks. *Chem. Soc. Rev.* **2012**, *41*, (2), 909-930.
6. Matsumiya, Y.; Watanabe, H.; Urakawa, O.; Inoue, T. Experimental Test for Viscoelastic Relaxation of Polyisoprene Undergoing Monofunctional Head-to-Head Association and Dissociation. *Macromolecules* **2016**, *49*, 7088-7095.
7. Callies, X.; Fonteneau, C.; Véchambre, C.; Pensec, S.; Chenal, J. M.; Chazeau, L.; Bouteiller, L.; Ducouret, G.; Creton, C. Linear rheology of bis-urea functionalized supramolecular poly(butylacrylate)s: Part I – weak stickers. *Polymer* **2015**, *69*, 233-240.
8. Fox, J. D.; Rowan, S. J. Supramolecular Polymerizations and Main-Chain Supramolecular Polymers. *Macromolecules* **2009**, *42*, (18), 6823-6835.
9. Yan, T.; Schröter, K.; Herbst, F.; Binder, W. H.; Thurn-Albrecht, T. What Controls the Structure and the Linear and Nonlinear Rheological Properties of Dense, Dynamic Supramolecular Polymer Networks? *Macromolecules* **2017**.
10. Yan, T.; Schröter, K.; Herbst, F.; Binder, W. H.; Thurn-Albrecht, T. Nanostructure and Rheology of Hydrogen-Bonding Telechelic Polymers in the Melt: From Micellar Liquids and Solids to Supramolecular Gels. *Macromolecules* **2014**, *47*, (6), 2122-2130.
11. Shabbir, A.; Goldansaz, H.; Hassager, O.; van Ruymbeke, E.; Alvarez, N. J. Effect of Hydrogen Bonding on Linear and Nonlinear Rheology of Entangled Polymer Melts. *Macromolecules* **2015**, *48*, (16), 5988-5996.
12. Lewis, C. L.; Stewart, K.; Anthamatten, M. The Influence of Hydrogen Bonding Side-Groups on Viscoelastic Behavior of Linear and Network Polymers. *Macromolecules* **2014**, *47*, (2), 729-740.
13. Ahmadi, M.; Hawke, L. G. D.; Goldansaz, H.; van Ruymbeke, E. Dynamics of Entangled Linear Supramolecular Chains with Sticky Side Groups: Influence of Hindered Fluctuations. *Macromolecules* **2015**, *48*, (19), 7300-7310.
14. Osterwinter, C.; Schubert, C.; Tonhauser, C.; Wilms, D.; Frey, H.; Friedrich, C. Rheological Consequences of Hydrogen Bonding: Linear Viscoelastic Response of Linear Polyglycerol and Its Permethylated Analogues as a General Model for Hydroxyl-Functional Polymers. *Macromolecules* **2015**, *48*, (1), 119-130.
15. Goldansaz, H.; Fustin, C.-A.; Wübbenhorst, M.; van Ruymbeke, E. How Supramolecular Assemblies Control Dynamics of Associative Polymers: Toward a General Picture. *Macromolecules* **2016**, *49*, (5), 1890-1902.
16. Krutyeva, M.; Brás, A.; Antonius, W.; Hövelmann, C.; Poulos, A.; Allgaier, J.; Radulescu, A.; Lindner, P.; Pyckhout-Hintzen, W.; Wischnewski, A. Association Behavior, Diffusion, and Viscosity of End-Functionalized Supramolecular Poly (ethylene glycol) in the Melt State. *Macromolecules* **2015**, *48*, (24), 8933-8946.
17. Staropoli, M.; Raba, A.; Hövelmann, C. H.; Krutyeva, M.; Allgaier, J.; Appavou, M.-S.; Keiderling, U.; Stadler, F. J.; Pyckhout-Hintzen, W.; Wischnewski, A.; Richter, D. Hydrogen Bonding in a Reversible

- Comb Polymer Architecture: A Microscopic and Macroscopic Investigation. *Macromolecules* **2016**, *49*, (15), 5692-5703.
18. Scavuzzo, J.; Tomita, S.; Cheng, S.; Liu, H.; Gao, M.; Kennedy, J. P.; Sakurai, S.; Cheng, S. Z. D.; Jia, L. Supramolecular Elastomers: Self-Assembling Star-Blocks of Soft Polyisobutylene and Hard Oligo(β -alanine) Segments. *Macromolecules* **2015**, *48*, (4), 1077-1086.
 19. Cao, P. F.; Li, B.; Hong, T.; Townsend, J.; Qiang, Z.; Xing, K.; Vogiatzis, K. D.; Wang, Y.; Mays, J. W.; Sokolov, A. P. Superstretchable, Self - Healing Polymeric Elastomers with Tunable Properties. *Adv. Funct. Mater.* **2018**, 1800741.
 20. Hackelbusch, S.; Rossow, T.; van Assenbergh, P.; Seiffert, S. Chain Dynamics in Supramolecular Polymer Networks. *Macromolecules* **2013**, *46*, (15), 6273-6286.
 21. Winter, A.; Schubert, U. S. Synthesis and characterization of metallo-supramolecular polymers. *Chem. Soc. Rev.* **2016**, *45*, (19), 5311-5357.
 22. Nair, K. P.; Pollino, J. M.; Weck, M. Noncovalently functionalized block copolymers possessing both hydrogen bonding and metal coordination centers. *Macromolecules* **2006**, *39*, (3), 931-940.
 23. Chen, Q.; Huang, C.; Weiss, R.; Colby, R. H. Viscoelasticity of reversible gelation for ionomers. *Macromolecules* **2015**, *48*, (4), 1221-1230.
 24. Stadler, F. J.; Pyckhout-Hintzen, W.; Schumers, J.-M.; Fustin, C.-A.; Gohy, J.-F. o.; Bailly, C. Linear Viscoelastic Rheology of Moderately Entangled Telechelic Polybutadiene Temporary Networks. *Macromolecules* **2009**, *42*, (16), 6181-6192.
 25. Lokey, R. S.; Iverson, B. L. Synthetic molecules that fold into a pleated secondary structure in solution. *Nature* **1995**, *375*, (6529), 303-305.
 26. Balkenende, D. W.; Coulibaly, S.; Balog, S.; Simon, Y. C.; Fiore, G. L.; Weder, C. Mechanochemistry with metallosupramolecular polymers. *J. Am. Chem. Soc.* **2014**, *136*, (29), 10493-10498.
 27. You, L.; Zha, D.; Anslyn, E. V. Recent advances in supramolecular analytical chemistry using optical sensing. *Chem. Rev.* **2015**, *115*, (15), 7840-7892.
 28. Bae, Y.; Fukushima, S.; Harada, A.; Kataoka, K. Design of environment - sensitive supramolecular assemblies for intracellular drug delivery: Polymeric micelles that are responsive to intracellular pH change. *Angew. Chem. Int. Ed.* **2003**, *42*, (38), 4640-4643.
 29. Sottos, N. R.; Moore, J. S. Materials chemistry: spot-on healing. *Nature* **2011**, *472*, (7343), 299-300.
 30. Cordier, P.; Tournilhac, F.; Soulie-Ziakovic, C.; Leibler, L. Self-healing and thermoreversible rubber from supramolecular assembly. *Nature* **2008**, *451*, (7181), 977-980.
 31. Yan, T.; Schröter, K.; Herbst, F.; Binder, W. H.; Thurn-Albrecht, T. Unveiling the molecular mechanism of self-healing in a telechelic, supramolecular polymer network. *Scientific Reports* **2016**, *6*.
 32. Xie, T. Tunable polymer multi-shape memory effect. *Nature* **2010**, *464*, (7286), 267-270.
 33. Lendlein, A.; Jiang, H.; Jünger, O.; Langer, R. Light-induced shape-memory polymers. *Nature* **2005**, *434*, (7035), 879-882.
 34. Murray, T. J.; Zimmerman, S. C. New triply hydrogen bonded complexes with highly variable stabilities. *J. Am. Chem. Soc.* **1992**, *114*, (10), 4010-4011.
 35. Quinn, J. R.; Zimmerman, S. C.; Del Bene, J. E.; Shavitt, I. Does the A-T or G-C Base-Pair Possess Enhanced Stability? Quantifying the Effects of CH \cdots O Interactions and Secondary Interactions on Base-Pair Stability Using a Phenomenological Analysis and ab Initio Calculations. *J. Am. Chem. Soc.* **2007**, *129*, (4), 934-941.
 36. Sijbesma, R. P.; Beijer, F. H.; Brunsveld, L.; Folmer, B. J.; Hirschberg, J. K.; Lange, R. F.; Lowe, J. K.; Meijer, E. Reversible polymers formed from self-complementary monomers using quadruple hydrogen bonding. *Science* **1997**, *278*, (5343), 1601-1604.

37. Chang, S. K.; Hamilton, A. D. Molecular recognition of biologically interesting substrates: synthesis of an artificial receptor for barbiturates employing six hydrogen bonds. *J. Am. Chem. Soc.* **1988**, *110*, (4), 1318-1319.
38. Cates, M. E. Reptation of living polymers: dynamics of entangled polymers in the presence of reversible chain-scission reactions. *Macromolecules* **1987**, *20*, 2289-2296.
39. Leibler, L.; Rubinstein, M.; Colby, R. H. Dynamics of reversible networks. *Macromolecules* **1991**, *24*, (16), 4701-4707.
40. Rubinstein, M.; Semenov, A. N. Thermoreversible gelation in solutions of associating polymers. 2. Linear dynamics. *Macromolecules* **1998**, *31*, (4), 1386-1397.
41. Rubinstein, M.; Semenov, A. N. Dynamics of entangled solutions of associating polymers. *Macromolecules* **2001**, *34*, 1058-1068.
42. Semenov, A. N.; Rubinstein, M. Thermoreversible gelation in solutions of associative polymers. 1. Statics. *Macromolecules* **1998**, *31*, (4), 1373-1385.
43. Semenov, A. N.; Rubinstein, M. Dynamics of entangled associating polymers with large aggregates. *Macromolecules* **2002**, *35*, 4821-4837.
44. Chen, Q.; Tudryn, G. J.; Colby, R. H. Ionomer dynamics and the sticky Rouse model. *J. Rheol.* **2013**, *57*, (5), 1441.
45. Gainaru, C.; Hiller, W.; Böhmer, R. A Dielectric Study of Oligo- and Poly(propylene glycol). *Macromolecules* **2010**, *43*, (4), 1907-1914.
46. Gainaru, C.; Böhmer, R. Oligomer-to-Polymer Transition of Poly(propylene glycol) Revealed by Dielectric Normal Modes. *Macromolecules* **2009**, *42*, (20), 7616-7618.
47. Dyre, J. C.; Olsen, N. B. Minimal model for Beta relaxation in viscous liquids. *Phys. Rev. Lett.* **2003**, *91*, (15), 155703.
48. Mattsson, J.; Bergman, R.; Jacobsson, P.; Borjesson, L. Chain-length-dependent relaxation scenarios in an oligomeric glass-forming system: from merged to well-separated alpha and beta loss peaks. *Phys. Rev. Lett.* **2003**, *90*, (7), 075702.
49. Grzybowska, K.; Grzybowski, A.; Ziolo, J.; Paluch, M.; Capaccioli, S. Dielectric secondary relaxations in polypropylene glycols. *J. Chem. Phys.* **2006**, *125*, (4), 44904.
50. Grzybowska, K.; Grzybowski, A.; Ziolo, J.; Rzoska, S. J.; Paluch, M. Anomalous behavior of secondary dielectric relaxation in polypropylene glycols. *J. Phys. Condens. Matter* **2007**, *19*, (37), 376105.
51. Pawlus, S.; Hensel-Bielowka, S.; Grzybowska, K.; Ziolo, J.; Paluch, M. Temperature behavior of secondary relaxation dynamics in tripropylene glycol. *Phys. Rev. B* **2005**, *71*, (17).
52. Ngai, K. L.; Pawlus, S.; Grzybowska, K.; Kaminski, K.; Capaccioli, S.; Paluch, M. Does the Johari-Goldstein β -Relaxation Exist in Polypropylene Glycols? *Macromolecules* **2015**, *48*, (12), 4151-4157.
53. Moon, I.; Jeong, Y.; Furukawa, T. Enthalpy and dielectric relaxation in the glass transition region of polypropylene glycol. *Thermochim. Acta* **2001**, *377*, (1-2), 97-104.
54. Hofmann, M.; Gainaru, C.; Cetinkaya, B.; Valiullin, R.; Fatkullin, N.; Rössler, E. Field-cycling relaxometry as a molecular rheology technique: common analysis of NMR, shear modulus and dielectric loss data of polymers vs dendrimers. *Macromolecules* **2015**, *48*, (20), 7521-7534.
55. Gainaru, C.; Hecksher, T.; Fan, F.; Xing, K.; Cetinkaya, B.; Olsen, N. B.; Dyre, J. C.; Sokolov, A. P.; Böhmer, R. Simple-liquid dynamics emerging in the mechanical shear spectra of poly (propylene glycol). *Colloid. Polym. Sci.* **2017**, *295*, (12), 2433-2437.
56. Cochrane, J.; Harrison, G.; Lamb, J.; Phillips, D. W. Creep, creep recovery and dynamic mechanical measurements of a poly(propylene glycol) oligomer. *Polymer* **1980**, *21*, 837-844.
57. Nicolai, T.; Floudas, G. Dynamics of linear and star poly (oxypropylene) studied by dielectric spectroscopy and rheology. *Macromolecules* **1998**, *31*, (8), 2578-2585.
58. Swenson, J.; Köper, I.; Telling, M. Dynamics of propylene glycol and its 7-mer by neutron scattering. *J. Chem. Phys.* **2002**, *116*, (12), 5073-5079.

59. Wang, C.-H.; Fytas, G.; Lilge, D.; Dorfmueller, T. Laser light beating spectroscopic studies of dynamics in bulk polymers: poly (propylene glycol). *Macromolecules* **1981**, *14*, (5), 1363-1370.
60. Engberg, D.; Schüller, J.; Strube, B.; Sokolov, A.; Torell, L. Brillouin scattering and dielectric relaxation in PPG of different chain lengths and end groups. *Polymer* **1999**, *40*, (17), 4755-4761.
61. Eckert, S.; Meier, G.; Alig, I. Phase behaviour of mixtures of polyethylene glycol and polypropylene glycol: Influence of hydrogen bond clusters on the phase diagram. *Phys. Chem. Chem. Phys.* **2002**, *4*, (15), 3743-3749.
62. Kaminski, K.; Kipnusu, W.; Adrjanowicz, K.; Mapesa, E.; Iacob, C.; Jasiurkowska, M.; Wlodarczyk, P.; Grzybowska, K.; Paluch, M.; Kremer, F. Comparative study on the molecular dynamics of a series of polypropylene glycols. *Macromolecules* **2013**, *46*, (5), 1973-1980.
63. Brás, A. R.; Hövelmann, C. H.; Antonius, W.; Teixeira, J.; Radulescu, A.; Allgaier, J.; Pyckhout-Hintzen, W.; Wischnewski, A.; Richter, D. Molecular Approach to Supramolecular Polymer Assembly by Small Angle Neutron Scattering. *Macromolecules* **2013**, *46*, (23), 9446-9454.
64. Cortese, J.; Soulie-Ziakovic, C.; Tence-Girault, S.; Leibler, L. Suppression of mesoscopic order by complementary interactions in supramolecular polymers. *J. Am. Chem. Soc.* **2012**, *134*, (8), 3671-4.
65. Cortese, J.; Soulié-Ziakovic, C.; Cloitre, M.; Tencé-Girault, S.; Leibler, L. Order–Disorder Transition in Supramolecular Polymers. *J. Am. Chem. Soc.* **2011**, *133*, (49), 19672-19675.
66. Xing, K.; Chatterjee, S.; Saito, T.; Gainaru, C.; Sokolov, A. P. Impact of Hydrogen Bonding on Dynamics of Hydroxyl-Terminated Polydimethylsiloxane. *Macromolecules* **2016**, *49*, (8), 3138-3147.
67. Xing, K.; Tress, M.; Cao, P.; Cheng, S.; Saito, T.; Novikov, V. N.; Sokolov, A. P. Hydrogen-bond strength changes network dynamics in associating telechelic PDMS. *Soft Matter* **2018**.
68. Ferry, A. Ionic interactions and transport properties in methyl terminated poly (propylene glycol)(4000) complexed with LiCF₃SO₃. *J. Phys. Chem. B* **1997**, *101*, (2), 150-157.
69. Ferry, A.; Tian, M. Influence of hydroxyl terminal groups on the ionic speciation and ionic conductivity in complexes of poly (propylene glycol)(4000) and LiCF₃SO₃ salt. *Macromolecules* **1997**, *30*, (4), 1214-1215.
70. Wagner, H.; Richert, R. Equilibrium and non-equilibrium type β -relaxations: D-sorbitol versus o-terphenyl. *J. Phys. Chem. B* **1999**, *103*, (20), 4071-4077.
71. Kunal, K.; Robertson, C. G.; Pawlus, S.; Hahn, S. F.; Sokolov, A. P. Role of chemical structure in fragility of polymers: a qualitative picture. *Macromolecules* **2008**, *41*, (19), 7232-7238.
72. Kaminski, K.; Kipnusu, W. K.; Adrjanowicz, K.; Mapesa, E. U.; Iacob, C.; Jasiurkowska, M.; Wlodarczyk, P.; Grzybowska, K.; Paluch, M.; Kremer, F. Comparative Study on the Molecular Dynamics of a Series of Polypropylene Glycols. *Macromolecules* **2013**, *46*, (5), 1973-1980.
73. Callies, X.; Véchambre, C.; Fonteneau, C.; Pensec, S.; Chenal, J. M.; Chazeau, L.; Bouteiller, L.; Ducouret, G.; Creton, C. Linear Rheology of Supramolecular Polymers Center-Functionalized with Strong Stickers. *Macromolecules* **2015**, *48*, (19), 7320-7326.
74. Hintermeyer, J.; Herrmann, A.; Kahlau, R.; Goiceanu, C.; Rossler, E. Molecular weight dependence of glassy dynamics in linear polymers revisited. *Macromolecules* **2008**, *41*, (23), 9335-9344.
75. Fox Jr, T. G.; Flory, P. J. Second - order transition temperatures and related properties of polystyrene. I. Influence of molecular weight. *J. Appl. Phys.* **1950**, *21*, (6), 581-591.
76. Kremer, F. S., A., *Broadband dielectric spectroscopy*. Springer-Verlag, Berlin: 2002.
77. Adachi, K.; Kotaka, T. Dielectric normal mode relaxation. *Prog. Polym. Sci.* **1993**, *18*, (3), 585-622.
78. Stockmayer, W. H. Dielectric dispersion in solutions of flexible polymers. *Pure Appl. Chem.* **1967**, *15*, (3-4), 539-554.
79. Roland, C.; Psurek, T.; Pawlus, S.; Paluch, M. Segmental - and normal - mode dielectric relaxation of poly (propylene glycol) under pressure. *J. Polym. Sci., Part B: Polym. Phys.* **2003**, *41*, (23), 3047-3052.

80. Schlosser, E.; Schönhals, A. Relation between main-and normal-mode relaxation. A dielectric study on poly (propyleneoxide). *Application of Scattering Methods to the Dynamics of Polymer Systems* **1993**, 158-161.
81. Schüller, J.; Mel'Nichenko, Y. B.; Richert, R.; Fischer, E. W. Dielectric studies of the glass transition in porous media. *Phys. Rev. Lett.* **1994**, *73*, (16), 2224.
82. Schönhals, A.; Stauga, R. Broadband dielectric study of anomalous diffusion in a poly(propylene glycol) melt confined to nanopores. *J. Chem. Phys.* **1998**, *108*, (12), 5130-5136.
83. Hayakawa, T.; Adachi, K. Dielectric normal mode relaxation of undiluted poly (propylene glycol) s. *Polymer* **2001**, *42*, (4), 1725-1732.
84. Gainaru, C.; Bohmer, R. Oligomer-to-Polymer Transition of Poly (propylene glycol) Revealed by Dielectric Normal Modes. *Macromolecules* **2009**, *42*, (20), 7616-7618.
85. Vogel, H. Flüssigkeiten Das Temperaturabhängigkeitsgesetz der Viskosität von. *Phys Zeitschr* **1921**, *22*, 645-646.
86. Tammann, G.; Hesse, W., *Die Abhängigkeit der Viscositat von der Temperatur bei unterkühlten Flüssigkeiten*. Zeitschrift fur anorganische und allgemeine Chemie: 1926; Vol. 156, p 245-257.
87. Fulcher, G. S. Analysis of recent measurements of the viscosity of glasses. *J. Am. Ceram. Soc.* **1925**, *8*, (6), 339-355.
88. Dudowicz, J.; Freed, K. F.; Douglas, J. F. Fragility of glass-forming polymer liquids. *J. Phys. Chem. B* **2005**, *109*, (45), 21350-21356.
89. Dudowicz, J.; Freed, K. F.; Douglas, J. F. The glass transition temperature of polymer melts. *J. Phys. Chem. B* **2005**, *109*, (45), 21285-21292.
90. Wübbenhorst, M.; Van Turnhout, J. Analysis of complex dielectric spectra. I. One-dimensional derivative techniques and three-dimensional modelling. *J. Non-Cryst. Solids* **2002**, *305*, (1-3), 40-49.
91. Ge, S.; Tress, M.; Xing, K.; Cao, P.-F.; Cheng, S.; Saito, T.; Novikov, N. N.; Sokolov, A. P. Molecular Mechanism of Stress Relaxation in Associating Telechelic Polymers. [in preparation].
92. Kautz, H.; Van Beek, D.; Sijbesma, R. P.; Meijer, E. Cooperative end-to-end and lateral hydrogen-bonding motifs in supramolecular thermoplastic elastomers. *Macromolecules* **2006**, *39*, (13), 4265-4267.
93. Staropoli, M.; Raba, A.; Hövelmann, C. H.; Appavou, M.-S.; Allgaier, J.; Krutyeva, M.; Pyckhout-Hintzen, W.; Wischnewski, A.; Richter, D. Melt dynamics of supramolecular comb polymers: Viscoelastic and dielectric response. *J. Rheol.* **2017**, *61*, (6), 1185-1196.
94. Gold, B.; Hövelmann, C.; Lühmann, N.; Pyckhout-Hintzen, W.; Wischnewski, A.; Richter, D. The microscopic origin of the rheology in supramolecular entangled polymer networks. *J. Rheol.* **2017**, *61*, (6), 1211-1226.
95. Gold, B.; Hövelmann, C.; Lühmann, N.; Székely, N.; Pyckhout-Hintzen, W.; Wischnewski, A.; Richter, D. Importance of Compact Random Walks for the Rheology of Transient Networks. *ACS Macro Letters* **2017**, *6*, (2), 73-77.